Molecular-dynamics prediction of the thermal conductivity of thin InP nanowires: Similarities to Si

J. Carrete,[1] R. C. Longo,[1] L. M. Varela,[1] J. P. Rino,[2] and L. J. Gallego[1,*]

[1]*Departamento de Física de la Materia Condensada, Facultad de Física, Universidad de Santiago de Compostela, E-15782 Santiago de Compostela, Spain*

[2]*Departamento de Física, Universidade Federal de São Carlos, 13.565-905 São Carlos, São Paulo, Brazil*

(Received 8 January 2009; revised manuscript received 7 September 2009; published 2 October 2009)

We investigated the thermal conductivity of InP nanowires with diameters $d=0.83$, 1.66, 2.49, 3.32, 4.15, and 4.97 nm by means of molecular-dynamics simulations using a potential with two-body and three-body contributions. In the temperature range of 100–700 K, thermal conductivities of approximately 1.0–2.5 W/(K m) are predicted—1 to 2 orders of magnitude smaller than the corresponding bulk values, but about 1 order of magnitude larger than those suggested by previous predictions.

DOI: 10.1103/PhysRevB.80.155408 PACS number(s): 68.65.−k, 63.22.Gh, 65.80.+n, 66.70.−f

Quasi-one-dimensional semiconductor nanowires have in recent years attracted considerable research effort for both theoretical reasons—the desire to understand how electronic, optical, thermal, and mechanical properties are affected by the reduction of dimensionality—and with a view to the potential technological applications of these nanosystems (see, e.g., Refs. 1–3). In particular, information on the thermal conductivity of semiconductor nanowires is crucial for the development of new nanoelectronic and thermoelectric devices. Extremely high thermal conductivity is essential if nanowires are to be used as heat sinks in future nanochips,[4,5] and ultralow thermal conductivity [say <1 W/(K m)], in conjunction with high electrical conductivity and large Seebeck coefficients, if they are to form the basis of efficient thermoelectric refrigerators and power generators.[6–9]

Only for a few relatively thick nanowires has thermal conductivity been determined experimentally[10–15] and, because of their relevance to the semiconductor industry, much of this work has concerned Si nanowires.[10,14,15] Over the temperature range of 20–320 K, the thermal conductivities of Si nanowires with diameters of 22, 37, 56, and 115 nm are about 2 orders of magnitude smaller than those of bulk Si and decrease with decreasing nanowire diameter, a trend that is attributed to the concomitant increase in surface-volume ratio, which enhances the scattering of long-wavelength phonons (the dominant heat carriers) by the nanowire boundary.[10] The results of theoretical studies[16–18] and computer simulations[19–21] are in broad agreement with these experimental findings and their interpretation. For example, in the temperature range of 200–500 K, classical molecular-dynamics (MD) simulations of Si nanowires with square cross sections of side 1.61–5.35 nm, performed by Volz and Chen[19] with both free and rigid boundary conditions using the Green-Kubo method[22] in conjunction with the Stillinger-Weber (SW) model of Si-Si interactions,[23] found thermal conductivities of 1–5 W/(K m) (1–2 orders of magnitude smaller than the corresponding bulk value) that decreased with nanowire diameter. Interestingly, however, MD simulations using the direct method[22] with the SW potential[23] show that for tetrahedral Si nanowires oriented along the [111] direction thermal conductivity decreases as wire diameter is reduced from 7.7 to 3.4 nm, but then increases as diameter is reduced further to 1.46 nm; this is attributed to a more subtle phonon confinement effect manifested in the fact that the excited mode of lowest frequency and longest wavelength shifts to higher frequency.[21] The thermal conductivities of Si_{34}- and Si_{46}-clathrate nanowires increase with decreasing diameter over the whole range investigated (2–8 nm), though only very slightly;[21] the similar though more pronounced diameter dependence of the room-temperature specific heat of thin Si [111] nanowires that is predicted by lattice dynamics theory and MD/SW simulations[24] has likewise been attributed to the combination of phonon confinement and the increase in specific free-surface area.[24]

In the light of the above results, Si nanowires seem unlikely to be very suitable for the applications mentioned earlier, although room-temperature thermal conductivities of 0.75 W/(K m) have been achieved with heavily doped Si.[25] An alternative nanowire material that has attracted considerable attention is InP. InP nanowires have been synthesized by several methods[26–31] and their energy-band gaps and photoluminescence images and spectra have been determined experimentally.[32,33] Furthermore, *p*-type doped InP nanowires function as light-emitting diodes and field-effect transistors when assembled with *n*-type nanowires,[34,35] and the impurity state responsible for current flow in Zn-doped InP nanowires has been characterized[36] by first-principles calculations based on PARSEC,[37] a real-space implementation of density-functional theory and pseudopotentials. However, as far as we know, there have hitherto been no systematic experimental or computational studies of the thermal conductivity of InP nanowires, although theoretical calculations using phonon-dispersion relations based on the somewhat crude Harrison potential[38] have been performed for wires up to 10^4 nm thick at 300 K by Mingo and Broido[39] and Mingo.[40]

In the work described here, we investigated the thermal conductivity of hexagonal InP nanowires by means of classical MD simulations using a potential proposed by Branício and Rino[41] that, like the SW potential for Si[23] and the potentials developed by Vashishta and co-workers for other semiconductor materials,[42–45] comprises both two-body and three-body terms. This potential has proved to be very useful for interpreting the vibrational properties and structural

 ©2009 The American Physical Society

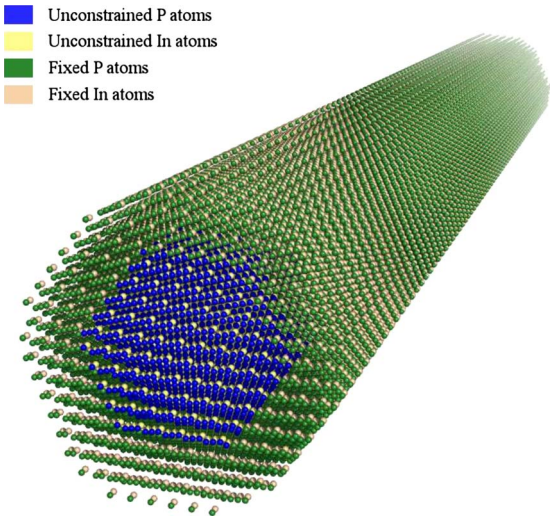

FIG. 1. (Color online) Schematic diagram of an InP nanowire excised from zinc blende-structured bulk InP in the [111] direction. In the case shown (d=4.15 nm), a central row of atoms is surrounded by five unconstrained atomic layers and three outer layers of atoms that were held fixed during simulations.

phase transformations of bulk InP under pressure,[41,46] but this is the first time that it has been applied to nanowires. Given the lack of systematic experimental studies of the thermal conductivity of InP nanowires, we compare our results to Mingo's theoretical results[39,40] and to experimental,[10,15] theoretical,[16–18] and computational[19–21] results for thin Si nanowires.

Our thermal-conductivity calculations employed direct simulations,[22] which unlike the Green-Kubo approach,[22] simulate experimental measurements by imposing a temperature gradient across the simulation cell; since this approach is faster than the Green-Kubo method (though providing similar results), it allows larger systems to be studied. We considered hexagonal InP nanowires cut from the zinc blende-structured bulk along the [111] direction (which was taken as the z axis). Each wire consisted of a central row of atoms together with between one and six surrounding atomic layers and this set of unconstrained atoms was itself surrounded by a further three layers of atoms that were held fixed during simulations (Fig. 1). These additional layers make the structure as a whole more similar to that of experimental wires, which have an amorphous coating, and were found to be necessary to ensure structural stability during simulations; they should also favor the applicability of the Branício-Rino potential,[41] which was developed for the bulk, by ensuring that every unconstrained atom has a bulklike environment (the cutoff radius of this potential extends to third nearest neighbors).

Each nanowire occupied a large supercell of length l =179 nm with periodic boundary conditions in the z direction so as to make the wire endless (increasing l further did not significantly alter the thermal conductivities calculated as described below). Heat flow was generated by establishing a temperature gradient along the z axis: with the cell centered at z=0, a hot thermostatic plate of width δ=10 nm was placed with its center at $z=-l/4$ and a cold one with its center at $z=l/4$. At each time step (of length dt), an amount of energy dE was added to the hot plate and the same amount was removed from the cold plate, in both cases by simply rescaling the velocities of the atoms in the plates relative to the centers of mass of the latter.[47] When the system reached a steady state, the heat flux per unit area and time was calculated as

$$J_z = \frac{dE}{2Adt}, \tag{1}$$

where A is the cross-sectional area of the wire (excluding the fixed surrounding layers) and the 2 in the denominator arises because, due to the periodic boundary conditions, heat flows in both directions from the hot plate to the cold plate. To calculate the temperature gradient dT/dz, the nanowire was notionally divided into 20 segments (ten on each side of the hot plate), their kinetic temperatures were averaged over 10^6 time steps after the steady state had been reached, the four segments containing the thermostats were "discarded" (with 20 segments, each thermostat is centered at the boundary between two segments), and a linear regression of segment temperature on the distance of the segment midpoint from the hot plate was performed. Fourier's law was then used to calculate the thermal conductivity as

$$\lambda = \frac{|J_z|}{|dT/dz|}. \tag{2}$$

Due to their computational demands, our MD simulations were necessarily restricted to nanowires of small diameter: the unconstrained parts of the wires with 1, 2, 3, 4, 5, and 6 unconstrained layers surrounding the central row of atoms have diameters of 0.83, 1.66, 2.49, 3.32, 4.15, and 4.97 nm, respectively. The total number of atoms (including the three fixed layers) ranged from 37 950 to 94 650. The MD simulations were performed using the velocity VERLET algorithm[48] with a time step dt=10 fs.

As noted above, the Branício-Rino potential consists of two-body and three-body terms.[41] The two-body terms represent steric repulsion, Coulomb interactions due to charge transfer, induced charge-dipole interactions, and van der Waals dipole-dipole interactions, while the three-body terms represent covalent bond bending and stretching. Although the parameters of the potential were not optimized for nanostructures, but using experimental values of properties of bulk InP (lattice constants, elastic moduli, cohesive energy, vibrational density of states, and parameters of the transition from the zinc blende to the rocksalt structure), it seems reasonable to assume that it is applicable to nanostructures with such large numbers of atoms as those simulated in the present work (whereas the transferability of bulk-derived potentials to small clusters of atoms or molecules is notoriously problematic; see, e.g., Refs. 49 and 50). The same assumption is made implicitly in studies of thin Si nanowires that use the SW potential with parameters optimized for prediction of the properties of bulk solid and liquid Si.[23]

For our InP nanowires with diameters d=1.66 and 4.15 nm, we computed thermal conductivities λ at temperatures T ranging from 100 to 700 K (Fig. 2). For most of this tem-

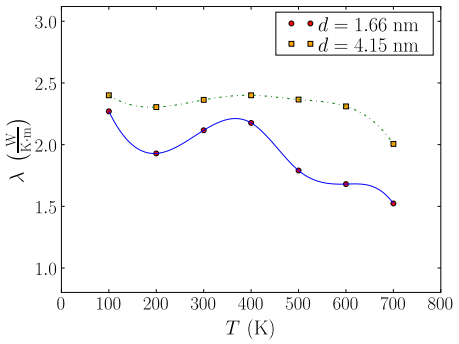

FIG. 2. (Color online) Thermal conductivities of InP nanowires of diameters $d=1.66$ and 4.15 nm as functions of temperature. The curves were obtained by fitting cubic splines to the data points (circles and squares).

perature range, the effects of phonon quantization, which are ignored by classical MD calculations, are negligible, although they may be significant at low temperatures. For the smaller diameter, $\lambda(T)$ falls overall from ≈ 2.3 W/(K m) at 100 K to ≈ 1.5 W/(K m) at 700 K, but has a local maximum of about 2.25 W/(K m) between 300 and 400 K. For the 4.15 nm InP wire, $\lambda(T)$ is almost flat over the range of 100–500 K and decreases monotonically from about 2.35 to 2.0 W/(K m) between 500 and 700 K. The computed thermal conductivities of both wires are similar to those calculated by Volz and Chen[19] for square nanowires of diamondlike Si of similar thickness in the range 200–500 K, 1–5 W/(K m); and for both our InP wires and Volz and Chen's Si wires, λ is 1–2 orders of magnitude smaller than for the corresponding bulk material [for bulk InP, $\lambda = 121$ W/(K m) at 200 K and 32 W/(K m) at 500 K;[51] for bulk Si,[19] $\lambda = 241$ W/(K m) at 200 K and 81 W/(K m) at 500 K]. Similarly, for clathrate Si nanowires of about 4 nm in diameter, Ponomareva *et al.*[21] calculated an almost flat $\lambda(T)$ with values of about 3–5 W/(K m) over the temperature range of 100–500 K. However, the $\lambda(T)$ calculated by Ponomareva *et al.*[21] for 4.2 nm wires of tetrahedral Si ranged from 18 to 30 W/(K m) and showed a maximum between 100 and 200 K, and was thus morphologically somewhat similar to the $\lambda(T)$ calculated in the present work for 1.66 nm InP nanowires, though with values and variation about 1 order of magnitude greater. The apparent discrepancy between the results of Volz and Chen[19] and Ponomareva *et al.*[21] for diamondlike Si wires seems likely to be due to the wires of the latter authors lying in the [111] direction of the bulk Si lattice, whereas Volz and Chen studied wires lying in the [110] direction.

Figure 3 shows the dependence of thermal conductivity on InP wire diameter at 100 and 300 K. At both temperatures, λ decreases monotonically as diameter is reduced from 4.97 to 2.49 nm. This behavior can be attributed to increased scattering of phonons by boundaries as the surface-to-volume ratio increases and is qualitatively in keeping both with the theoretical findings for InP wires up to 10^4 nm thick that were obtained by Mingo and Broido[39] and Mingo[40] using complete phonon-dispersion relations and Harrison's potential[38] and with results obtained for Si nanowires by experiment,[10,15] theoretical calculations,[16–18] and computer

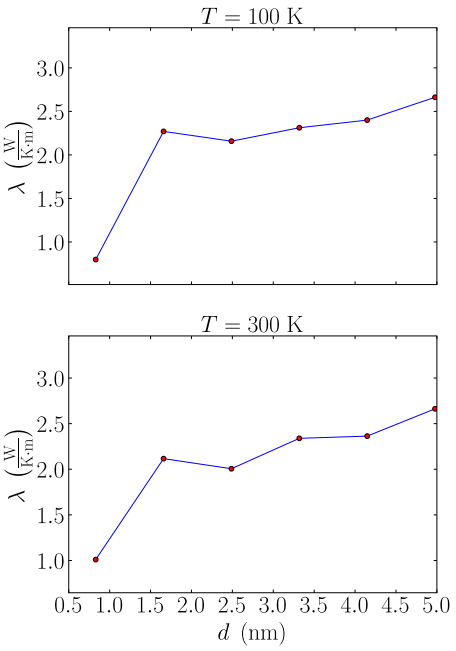

FIG. 3. (Color online) Diameter dependence of the thermal conductivity of InP nanowires at 100 and 300 K. The lines joining the data points are merely visual aids.

simulation.[19–21] However, the present values are about 1 order of magnitude larger than those predicted by extrapolation of the theoretical results of Mingo and Broido[39] for cylindrical InP wires at $T=300$ K. This difference, which significantly reduces the attractiveness of InP for the design of thermoelectric devices, is largely attributable to Mingo and Broido having employed a rather crude potential, Harrison's[38] (equivalent to the harmonic limit of an SW-like potential), no doubt partly because they wished to survey a number of different materials using the same potential and partly because there was in any case no InP-specific potential available at that time. Indeed, simulations of InP nanowires of the same sizes as in the present study, carried out at 300 K using Harrison's potential with the same parameterization as was used by Mingo and Broido, afford conductivities similar to those suggested by extrapolation of Mingo and Broido's theoretical values (results not shown).

Further reduction of the wire diameter from 2.49 to 1.66 nm causes λ to increase slightly, after which it falls abruptly to 0.8–1.0 W/(K m) for $d=0.83$ nm (at which value the central one-dimensional row of atoms has just one unconstrained atomic layer surrounding it). Following Ponomareva *et al.*,[21] who found the thermal conductivities of tetrahedral Si nanowires to increase with decreasing wire thickness at thicknesses <3 nm, we investigated the similarly inverted thickness dependence of the thermal conductivity of InP wires at $d=1.66$ nm by computing the phonon spectra of the four smallest nanowires at 100 and 300 K. The spectra were calculated as the Fourier transforms (FTs) of the normalized velocity autocorrelation function $Z(t) = \langle \mathbf{v}_i(t) \cdot \mathbf{v}_i(0) \rangle / \langle \mathbf{v}_i(0) \cdot \mathbf{v}_i(0) \rangle$, which was generated in a 10^5-step simulation with $dt=1$ fs (angle brackets denote an ensemble average). Figure 4 shows the spectral densities obtained at 100 K in the low-frequency (0–7 THz) region (the

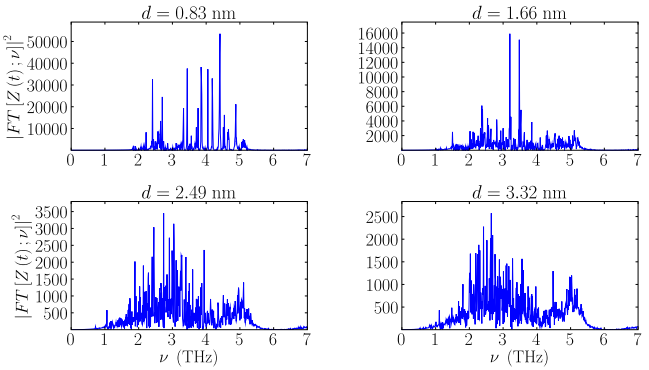

FIG. 4. (Color online) Low-frequency phonon spectra calculated at $T=100$ K for InP nanowires of several diameters.

region where thermal conductivity is largely determined), and the frequencies of the main peaks in this region are listed in Table I (the results for 300 K are similar). That the spectral density of the 0.83 nm wire is less than those of the others in this region clearly explains its markedly smaller thermal conductivity and is attributable to this wire having fewer atoms than the others. The local maximum of λ at 1.66 nm may be related not only to the marked overall increase in spectral intensity as diameter decreases (observe the vertical axes of the graphs of Fig. 4), but also to the shift of the two most excited modes from 2.48 and 2.62 THz to 3.16 and 3.46 THz as diameter decreases from 3.32 to 1.66 nm; this shift seems to indicate a local alteration of the dispersion relations that might increase the energy borne by this mode, possibly through its effect on the group velocity.

To sum up, we have investigated the thermal conductivity λ of very thin [111] zinc blende-structured InP nanowires by means of MD simulations using the direct method in conjunction with the potential developed by Branício and Rino[41] for bulk InP. In the temperature range of 100–700 K, the computed thermal conductivities are 1–2 orders of magnitude smaller than the corresponding bulk values (but about 1 order of magnitude larger than those suggested by previous predictions[39]) and plots of λ against wire diameter d at 100 and 300 K show a small local maximum at $d=1.66$ nm that appears to be related to a shift of the two most excited phonon modes to higher frequencies. In both these respects, InP [111] nanowires resemble [111] tetrahedral Si nanowires. The range of calculated thermal conductivities, approximately 1–2.5 W/(K m), suggests that InP nanowires are not suitable for use either as heat sinks or in thermoelectric devices.

TABLE I. Frequencies of the main peaks in the spectra of Fig. 4. For $d=1.66$, 2.49, and 3.32 nm, the frequencies of the two most excited modes are shown in bold.

Diameter (nm)	Peak frequencies (THz)
0.83	2.37, 3.41, 3.83, 4.03, 4.15, 4.4, 4.86, 4.8–5.0
1.66	2.37, **3.16**, **3.46**, 3.83, 4.5–5.5
2.49	1.84, 2.37, 2.48, **2.72**, **2.89**, 3.25, 3.50, 3.83, 4.5–5.5
3.32	2.00, 2.15–2.30, 2.38, **2.48**, **2.62**, 3.25, 3.54, 4.5–5.5

We are grateful to M. M. G. Alemany for useful discussions. This work was supported by the Spanish Ministry of Science and Innovation in conjunction with the European Regional Development Fund (Grant No. FIS2008-04894/FIS) and by the Directorate General for R+D+i of the Xunta de Galicia (Grants No. INCITE08E1R206041ES and No. INCITE08PXIB206107PR). J.C. thanks the Spanish Ministry of Science and Innovation for an FPU grant. Facilities provided by the Galician Supercomputing Centre (CESGA) are also acknowledged.

*Corresponding author. luisjavier.gallego@usc.es

[1] Y. Xia, P. Yang, Y. Sun, Y. Wu, B. Mayers, B. Gates, Y. Yin, F. Kim, and H. Yan, Adv. Mater. **15**, 353 (2003).
[2] M. Law, J. Goldberger, and P. Yang, Annu. Rev. Mater. Res. **34**, 83 (2004).
[3] W. Kim, R. Wang, and A. Majumdar, Nanotoday **2**, 40 (2007).
[4] J. Zou and A. Balandin, Proc. Electrochem. Soc. **2001-19**, 70 (2001).
[5] P. K. Schelling, L. Shi, and K. E. Goodson, Mater. Today **8**, 30 (2005).
[6] L. D. Hicks and M. S. Dresselhaus, Phys. Rev. B **47**, 12727 (1993).
[7] G. Mahan, B. Sales, and J. Sharp, Phys. Today **50**(3), 42 (1997).
[8] G. S. Nolas, J. Sharp, and H. J. Goldsmid, *Thermoelectrics* (Springer, New York, 2001).
[9] A. Majumdar, Science **303**, 777 (2004).
[10] D. Li, Y. Wu, P. Kim, L. Shi, P. Yang, and A. Majumdar, Appl. Phys. Lett. **83**, 2934 (2003).
[11] D. Li, Y. Wu, R. Fan, P. Yang, and A. Majumdar, Appl. Phys. Lett. **83**, 3186 (2003).
[12] J. Zhou, C. Jin, J. H. Seol, X. Li, and L. Shi, Appl. Phys. Lett. **87**, 133109 (2005).
[13] L. Shi, Q. Hao, C. Yu, N. Mingo, X. Kong, and Z. L. Wang, Appl. Phys. Lett. **84**, 2638 (2004).
[14] O. Bourgeois, T. Fournier, and J. Chaussy, J. Appl. Phys. **101**, 016104 (2007).
[15] R. Chen, A. I. Hochbaum, P. Murphy, J. Moore, P. Yang, and A. Majumdar, Phys. Rev. Lett. **101**, 105501 (2008).
[16] N. Mingo, Phys. Rev. B **68**, 113308 (2003).
[17] N. Mingo, L. Yang, D. Li, and A. Majumdar, Nano Lett. **3**, 1713 (2003).
[18] P. Chantrenne, J. L. Barrat, X. Blase, and J. D. Gale, J. Appl. Phys. **97**, 104318 (2005).
[19] S. G. Volz and G. Chen, Appl. Phys. Lett. **75**, 2056 (1999).
[20] Y. Chen, D. Li, J. R. Lukes, and A. Majumdar, ASME J. Heat Transfer **127**, 1129 (2005).

[21] I. Ponomareva, D. Srivastava, and M. Menon, Nano Lett. **7**, 1155 (2007).
[22] P. K. Schelling, S. R. Phillpot, and P. Keblinski, Phys. Rev. B **65**, 144306 (2002).
[23] F. H. Stillinger and T. A. Weber, Phys. Rev. B **31**, 5262 (1985); **33**, E1451 (1986).
[24] Y. Zhang, J. X. Cao, Y. Xiao, and X. H. Yan, J. Appl. Phys. **102**, 104303 (2007).
[25] A. I. Boukai, Y. Bunimovich, J. Tahir-Kheli, J.-K. Yu, W. A. Goddard III, and J. R. Heath, Nature (London) **451**, 168 (2008).
[26] T. J. Trentler, K. M. Hickman, S. C. Goel, A. M. Viano, P. C. Gibbons, and W. E. Buhro, Science **270**, 1791 (1995).
[27] T. J. Trentler, S. C. Goel, K. M. Hickman, A. M. Viano, M. Y. Chiang, A. M. Beatty, P. C. Gibbons, and W. E. Buhro, J. Am. Chem. Soc. **119**, 2172 (1997).
[28] X. F. Duan and C. M. Lieber, Adv. Mater. **12**, 298 (2000).
[29] M. S. Gudiksen and C. M. Lieber, J. Am. Chem. Soc. **122**, 8801 (2000).
[30] M. S. Gudiksen, J. F. Wang, and C. M. Lieber, J. Phys. Chem. B **105**, 4062 (2001).
[31] C. Tang, Y. Bando, Z. Liu, and D. Golberg, Chem. Phys. Lett. **376**, 676 (2003).
[32] H. Yu, J. Li, R. A. Loomis, L.-W. Wang, and W. E. Buhro, Nature Mater. **2**, 517 (2003).
[33] M. S. Gudiksen, J. Wang, and C. M. Lieber, J. Phys. Chem. B **106**, 4036 (2002).
[34] Y. Huang and C. M. Lieber, Pure Appl. Chem. **76**, 2051 (2004).
[35] X. F. Duan, Y. Huang, Y. Cui, J. Wang, and C. M. Lieber, Nature (London) **409**, 66 (2001).
[36] M. M. G. Alemany, X. Huang, M. L. Tiago, L. J. Gallego, and J. R. Chelikowsky, Nano Lett. **7**, 1878 (2007).
[37] M. M. G. Alemany, M. Jain, L. Kronik, and J. R. Chelikowsky, Phys. Rev. B **69**, 075101 (2004); M. M. G. Alemany, M. Jain, M. L. Tiago, Y. Zhou, Y. Saad, and J. R. Chelikowsky, Comput. Phys. Commun. **177**, 339 (2007).
[38] W. A. Harrison, *Electronic Structure and the Properties of Solids* (Dover, New York, 1989).
[39] N. Mingo and D. A. Broido, Phys. Rev. Lett. **93**, 246106 (2004).
[40] N. Mingo, Appl. Phys. Lett. **84**, 2652 (2004); **88**, 149902(E) (2006).
[41] P. S. Branício and J. P. Rino, Phys. Status Solidi B **244**, 331 (2007).
[42] P. Vashishta, R. K. Kalia, J. P. Rino, and I. Ebbsjö, Phys. Rev. B **41**, 12197 (1990).
[43] F. Shimojo, I. Ebbsjö, R. K. Kalia, A. Nakano, J. P. Rino, and P. Vashishta, Phys. Rev. Lett. **84**, 3338 (2000).
[44] J. P. Rino, A. Chatterjee, I. Ebbsjö, R. K. Kalia, A. Nakano, F. Shimojo, and P. Vashishta, Phys. Rev. B **65**, 195206 (2002).
[45] P. S. Branício, R. K. Kalia, A. Nakano, J. P. Rino, F. Shimojo, and P. Vashishta, Appl. Phys. Lett. **82**, 1057 (2003).
[46] J. P. Rino and P. S. Branício, Phys. Status Solidi B **244**, 239 (2007).
[47] P. Jund and R. Jullien, Phys. Rev. B **59**, 13707 (1999).
[48] M. P. Allen and D. J. Tildesley, *Computer Simulation of Liquids* (Oxford University Press, Oxford, 1990).
[49] C. Rey, L. J. Gallego, J. García-Rodeja, J. A. Alonso, and M. P. Iñiguez, Phys. Rev. B **48**, 8253 (1993).
[50] J. García-Rodeja, C. Rey, L. J. Gallego, and J. A. Alonso, Phys. Rev. B **49**, 8495 (1994).
[51] S. A. Aliev, A. Y. Nashelskii, and S. S. Shalyt, Sov. Phys. Solid State **7**, 1287 (1965).